Crystal and electronic structures of pentacene thin films from grazing-incidence x-ray diffraction and first-principles calculations

Dmitrii Nabok,* Peter Puschnig, and Claudia Ambrosch-Draxl
Chair for Atomistic Modelling and Design of Materials, Montanuniversität Leoben, Franz-Josef-Straße 18, A-8700 Leoben, Austria†

Oliver Werzer and Roland Resel
Institute of Solid State Physics, Graz University of Technology, Petersgasse 16, A-8010 Graz, Austria

Detlef-M. Smilgies
CHESS Centre, Cornell University, Ithaca, New York 14853, USA

(Received 26 June 2007; revised manuscript received 19 September 2007; published 21 December 2007)

Combined experimental and theoretical investigations on thin films of pentacene are performed in order to determine the structure of the pentacene thin film phase. Grazing incidence x-ray diffraction is used for studying a pentacene thin film with a nominal thickness of 180 nm. The crystal structure is found to exhibit the lattice parameters $a=0.592$ nm, $b=0.754$ nm, $c=1.563$ nm, $\alpha=81.5°$, $\beta=87.2°$, and $\gamma=89.9°$. These crystallographic unit cell dimensions are used as the only input parameters for *ab initio* total-energy calculations within the framework of density functional theory revealing the molecular packing within the crystal structure. Moreover, we calculate the electronic band structure of the thin film phase and compare it to that of the bulk phase. We find the intermolecular bandwidths of the thin film phase to be significantly larger compared to the bulk structure, e.g., the valence bandwidth is twice as large. This remarkable effect is traced back to an enhanced intermolecular π-π overlap due to the upright standing molecules in the thin film phase.

DOI: 10.1103/PhysRevB.76.235322 PACS number(s): 71.15.Nc, 61.66.Hq, 71.15.Mb, 61.10.−i

I. INTRODUCTION

Pentacene is one of the most prominent materials used in organic electronics. The high reproducibility of thin films by vacuum deposition of the molecules combined with good electronic performance make it a perfect material for studying the basic properties of an organic electronic device.[1] The modification of process parameters together with the variations of substrates opens the possibility to study the basic properties of an organic thin film transistor from the monolayer to the bulk.

The growth of the pentacene films shows a variety of crystalline phases where three different polymorphic structures have been reported.[2,3] Only for two structures, namely, the Campbell or "bulk" phase[4] and the so-called "single crystal" phase,[5,6] a complete structural solution is known. Although the thin film phase is crucial for the charge transport within thin film transistors, the geometry of the *thin film* structure is still subject of ongoing research.[7,8] The reason is that it is only formed on isotropic surfaces and the subsequent appearance of a pentacene bulk phase[9,10] does not allow for the growth of single crystals of a size sufficient for a full structure solution. Moreover, isotropic surfaces such as silicon oxide or polymer surfaces lead to the formation of domains in the thin film phase with a preferred orientation of the crystallites with the crystallographic (001) plane oriented parallel to the substrate surface.[11,12] Recently, however, Yoshida *et al.* suggested a structure solution of the pentacene thin film phase by means of x-ray diffraction studies supported by empirical force field calculations.[7] A similar structure has also been reported by Schiefer *et al.* entirely from diffraction data[8] and is also in accordance with our findings. The focus of the current work lies not only on the crystal structure but also on the *electronic* structure of the pentacene thin film phase. Therefore, we have chosen a combined experimental and *ab initio* density functional theory (DFT) approach. This method allows us to overcome the experimental limitations mentioned above and has been proven successful for a variety of aromatic molecules.[13–16] We calculate the *ab initio* DFT band structure based on the structural solution reported herein and recently published.[7,8] In contrast, previous attempts to compute the band structure of the thin film phase[17,18] relied on assumptions about the crystal structure since the correct molecular orientation was not known. Our results also differ significantly from the band structure of bulk pentacene.[19–21] This is an important result since the thin film phase plays an important role for the charge transport in pentacene thin film transistors.

The paper is organized as follows. Section II summarizes the experimental details of film preparation and x-ray diffraction experiments and Sec. III gives computational details about our *ab initio* DFT approach. In Sec. IV A, we present the grazing incidence diffraction pattern and its indexation, while Secs. IV B and IV C provide details on the internal structure determination by DFT calculations and on the comparison between experimental and theoretical diffraction intensities. Section IV D discusses the electronic band structure of the pentacene thin film phase in comparison with the bulk phase. Section V finally contains a discussion of the results and our conclusions.

II. EXPERIMENTAL DETAILS

The pentacene thin film was prepared by physical vapor deposition on oxidized silicon substrates under high vacuum conditions (10^{-6} mbar) using a source temperature of

165 °C. During the deposition process the substrate temperature was kept at 60 °C and the nominal layer thickness was monitored by a quartz microbalance; a deposition rate of 0.1 nm/min was obtained.[22] A film with a thickness of 180 nm was selected for x-ray diffraction investigations at the beamline G2 at CHESS.[23] Specular scans and grazing incidence diffraction were performed by using radiation with a wavelength of 0.1318 nm. In the case of grazing incidence diffraction, an incidence angle of 0.15° was used in combination with a one-dimensional detector probing simultaneously all out-of-plane diffraction angles up to 8° with a resolution of 0.015°. The in-plane diffraction angle was varied by 0.02° steps and a counting time of 20 s was chosen.

III. METHODS OF CALCULATION

A. Computational details

Starting from the experimentally determined lattice parameters, we performed *ab initio* calculations with the PWSCF-ESPRESSO code.[24] We used ultrasoft pseudopotentials[25] with a plane wave energy cutoff of 40 Ry. Exchange and correlation effects were treated by the generalized gradient approximation.[26] For Brillouin zone integrations, we used the Monkhorst-Pack scheme[27] with a $4\times4\times3$ mesh. The band structure calculations were carried out for a path in the Brillouin zone connecting the high-symmetry points X, Γ, Y, C, and Z with the internal coordinates of these points being (0.5,0,0), (0,0,0), (0,0.5,0), (0.5,0.5,0), and (0,0,0.5) in units $(2\pi/a, 2\pi/b, 2\pi/c)$, respectively. Note that the $\overline{\Gamma Z}$ direction is normal to the **ab** plane, i.e., perpendicular to the pentacene layers. Since all triclinic angles are close to 90°, the $\overline{\Gamma X}$ and $\overline{\Gamma Y}$ directions are almost parallel to the crystal **ab** plane, that is, within the pentacene layers. For the calculation of the density of states (DOS), the **k**-space integration was performed by the improved tetrahedron method with a $6\times6\times4$ mesh.[28]

B. Internal geometry optimization

For all molecular crystals, one can distinguish between strong intramolecular and comparably weak intermolecular forces acting on the atoms. This fact allows us to divide the procedure of geometry relaxation into two steps. First, we relax the internal geometry of the pentacene molecules, and consequently, we optimize their orientation within the unit cell by considering, the molecules as rigid.

Pentacene ($C_{22}H_{14}$) crystallizes in the triclinic space group $P\bar{1}$. Two features are common for many organic molecular crystals. The first one is the herringbone stacking[29] of the two inequivalent planar rodlike molecules, and the second one is the formation of layers in the crystalline $\mathbf{c}^*$ direction, as depicted in Fig. 1. Pursuing the nomenclature of Ref. 30 for denoting the orientation of the molecules within the crystal unit cell, we have chosen the following angles. The herringbone angle θ defines the angle between the normal vectors of the molecular planes of two inequivalent molecules. The orientation of the long molecular axis is described by two polar angles, χ and ϕ, in the local coordinate system where the **z** axis is parallel to $\mathbf{c}^*$ [normal to the (**ab**) plane] and the **x** axis coincides with the crystal direction **a** (see Fig. 1). Triclinic symmetry requires four independent polar angles (two for each molecule). From the existing experimental structure data of the pentacene polymorphs, however, it is known that the angle between the long molecular axes (in our notation δ) does not exceed 1.5°.[3] Due to this fact, we only consider those geometries as a starting point for the geometry optimization, where the long molecular axes of both inequivalent molecules have the same orientation. The detailed procedure is outlined in the following: We first minimize the total energy of the crystal by rotating the inequivalent molecules around their respective long axes, i.e., by changing the herringbone angle and keeping the values of the polar angles constant. Subsequently, we fix the value of the herringbone angle corresponding to the minimum energy and successively change the angles χ and ϕ. As a final step for the internal geometry minimization, we relax the atomic positions such that the remaining forces are below 1 mRy/a.u. By doing so, the molecule as a whole is allowed to rotate by some small angle. Therefore, after this last relaxation step, the two inequivalent molecules do not necessarily have the same orientation of the long axes anymore leading to δ slightly deviating from 0°.

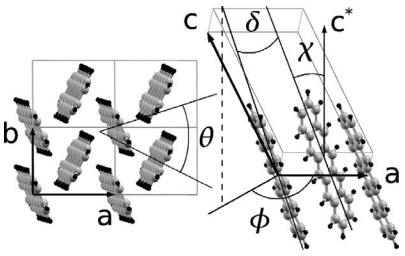

FIG. 1. Crystal structure of the pentacene crystal. The herringbone arrangement of the molecules in the (**ab**) plane and the orientation angles θ, χ, ϕ, and δ are shown.

IV. RESULTS

A. Experimental results

The specular x-ray diffraction scans reveal the typical diffraction features of a pentacene thin film grown on silicon oxide.[31,32] Two series of diffraction peaks are observed. The dominating ones arise from an interplanar distance $d_{001}=1.544\pm0.003$ nm which can be identified as the $00L$ peaks of the thin film structure. This observed value is in excellent agreement with literature data.[33] The second peak series is of much lower intensity and come from an interplanar distance of 1.443 ± 0.003 nm. This value does not fit to the "single crystal" structure obtained by Holmes *et al.*[5] and Siegrist,[6] but is close to $d_{001}=1.450$ nm of the "bulk" structure of Campbell *et al.*[4] The presence of the structure of Campbell *et al.* besides the thin film structure has already been proven experimentally.[34]

The grazing incidence diffraction studies reveal randomly distributed crystallites (two-dimensional powder). A typical diffraction pattern is depicted in Fig. 2. The diffraction peaks marked by crosses are calculated positions arising from the

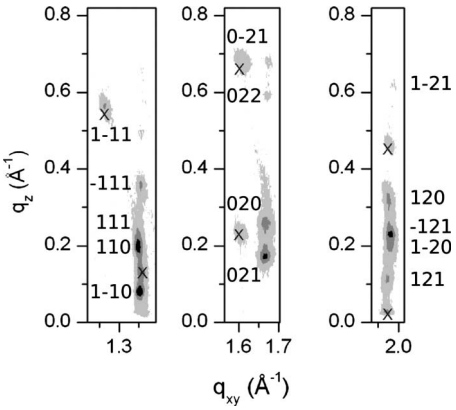

FIG. 2. Grazing incidence diffraction pattern of a 180 nm thick pentacene thin film, where the intensities of the diffraction spots are square-root scaled. Diffraction spots arising from the phase of Campbell *et al.* are marked by crosses. The indices of the diffraction peaks are given only for the thin film phase.

structure of Campbell *et al.* taking into account the preferred orientation of the crystallites. All expected diffraction peaks with sufficiently high intensity are observed which reveals that the structure of Campbell *et al.* is definitely present in the film.

The residual peaks could be used for an indexation of the pentacene thin film phase. Since the sample shows a strong (001) preferred orientation, the observed q_{xy} values of the diffraction peaks could be used to determine the Miller indices *hk* according to literature data.[35] Considering also the q_z part of the diffraction peaks, the complete indexation of *hkl* is obtained by determining the unit cell parameters of the reciprocal lattice. The fact that the length of the reciprocal unit cell vector $\mathbf{c}^*$ is known accurately from the specular scan simplifies the indexation procedure considerably.[36] The obtained lattice constants are $a=0.592$ nm, $b=0.754$ nm, $c=1.563$ nm, $\alpha=81.5°$, $\beta=87.2°$, and $\gamma=89.9°$ and are compared with those of the phase of Campbell *et al.* in Table I. The values are quite close to results obtained from electron diffraction on microcrystals[37] and they are in excellent agreement with results of other recent x-ray diffraction experiments.[7,8]

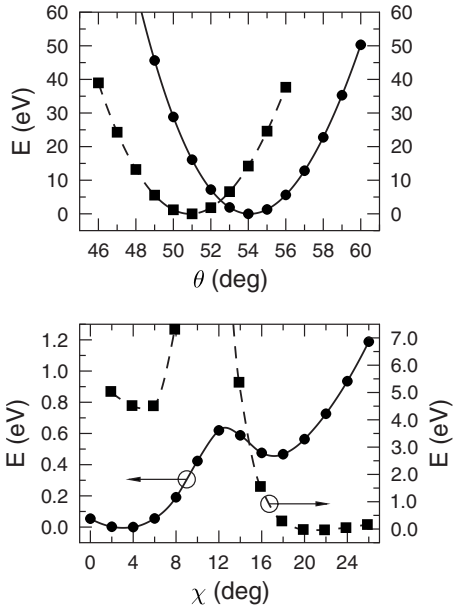

FIG. 3. Total energies of the thin film phase (solid line) and the bulk phase (dash line) polymorphs as a function of the herringbone θ (top) and the tilting χ angles (bottom). Origin of the energy scale shifted to the absolute energy minimum of the corresponding curve.

B. Internal geometry

To estimate the accuracy of our two-step procedure for the geometry optimization as described above, we tested the approach for the pentacene bulk structure for which the internal geometry is well known.[4] For this purpose, we placed two pentacene molecules in a unit cell with experimental lattice parameters determined by Campbell *et al.* Results of this procedure are plotted in Fig. 3, and the optimal values of the orientation angles are compiled in Table II. The comparison of the experimental and the optimized internal geometry shows good agreement and allows us to reliably apply this optimization procedure to the search for the internal geometry of the thin film phase. The lattice parameters of the thin film phase as measured by x-ray diffraction (Table I) are the only parameters entering the calculation leading to the internal geometry of the molecules in this phase. The results are

TABLE I. Triclinic lattice parameters *a*, *b*, *c*, α, β, and γ and the unitcell volume *V* of the thin film pentacene polymorph as determined from x-ray measurements. For comparison, the lattice constants of Refs. 7 and 8 as well as the bulk phase (Ref. 4) are given. A different choice of the unit cell vectors for the bulk phase with respect to Ref. 4 is used.

Phase Thin film	*a* (nm)	*b* (nm)	*c* (nm)	α (deg)	β (deg)	γ (deg)	*V* (nm^3)
This work	0.592	0.754	1.563	81.5	87.2	89.9	0.689
Yoshida *et al.*[a]	0.593	0.756	1.565	98.6	93.3	89.8	0.693
Schiefer *et al.*[b]	0.5958	0.7596	1.561	81.25	86.56	89.80	0.697
Bulk[c]	0.606	0.790	1.501	81.6	77.2	85.8	0.692

[a]Reference 7.
[b]Reference 8.
[c]Reference 4.

TABLE II. Calculated orientation angles of the molecules in bulk and thin film pentacene in comparison with the experimental data for the bulk phase. The total energies for both structures are shown in the last row.

	Bulk (expt)[a]	Bulk (opt)	Thin film (opt)
θ (deg)	52.5	50.9	54.1
χ_1 (deg)	22.4	21.9	3.1
χ_2 (deg)	20.5	20.9	2.9
δ (deg)	2.2	1.0	0.3
E_{total} (Ry)	−533.8978	−533.8976	−533.8973

[a]Reference 4.

given in Table II. The comparison with the bulk phase data shows the following characteristic features. First of all, there is a pronounced difference in the tilting angle χ which is $\approx 20°$ for the bulk and only $\approx 3°$ for the thin film phase. The main reason for this behavior can be found in the smaller interlayer separation of the bulk phase (1.45 nm) compared to the thin film phase (1.543 nm). On the other hand, the herringbone angle θ for the film phase 54° is close to the corresponding quantity for the olygoacene series ($\approx 52°$) where the a and b lattice parameters almost constant.

Another interesting feature is the dependence of the total energy on the tilting angle. The presence of two local minima, a first one at about 3° and a second one at roughly 18° for the thin film phase are clearly observed. This behavior is seen for the bulk phase as well, where the minima are located at $\approx 5°$ and $\approx 21°$. In contrast to the thin film phase, the deepest minimum is the second local minimum at a tilting angle of 22°. Moreover, different energy barriers between the minima are revealed. For the thin film phase, this barrier is about 0.4 eV, whereas for the bulk phase, it is an order of magnitude larger (about 5 eV). When we compare the total energies of the bulk and the thin film phase, we observe the energy difference to be only 6.5 meV which shows that both phases are likely to coexist in the films.

C. Comparison between theory and experiment

Based on the theoretically determined molecular packing, a diffraction pattern is computed and compared with line scans at constant q_{xy} of the experimental diffraction pattern in Fig. 4. The intensities are calculated with the assumption of randomly distributed crystallites.[38] In Fig. 4, the theoretical powder spectra for two different molecular orientations characterized by $\chi=3°$ (black bars) and $\chi=18°$ (gray bars) are compared with the experimental data (lines). We find an overall good agreement with experiment only for the theoretical intensities corresponding to the $\chi=3°$ orientation. In particular, the most pronounced diffraction peaks, namely, (1−10), (110), (021), and (020) strongly favor the 3° solution. At $\chi \approx 18°$, on the other hand, the (1−10), (110), and (021) reflections are considerably underestimated, while the (020) is predicted to be the highest in intensity. Also, the relative intensities of (1−10) vs (110) and (021) vs (020) are in excellent agreement only for the 3° structure, as predicted

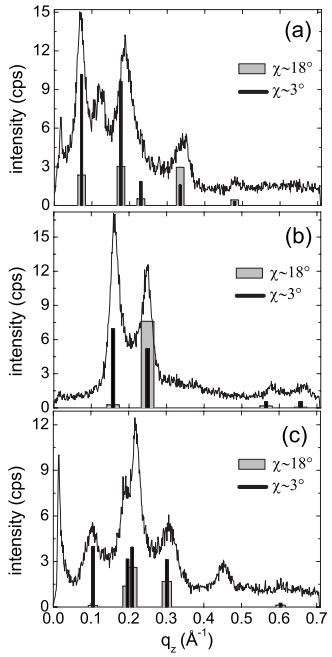

FIG. 4. Integrated diffraction intensities of Fig. 2 taken in the q_{xy} range (a) (1.33, 1.38), (b) (1.63, 1.70), and (c) (1.93, 2.01) and normalized to a single line scan. Calculated peak positions and relative intensities are given by bars for the two structural solutions $\chi \approx 3°$ and $\chi \approx 18°$.

from the DFT total energy optimization. There remain some small deviations between calculated and experimental intensities, e.g., the ratio between the (−121) and (121) peak heights [Fig. 4(c)]. This can be explained by the fact that the peak height of (121) is decreased due to peak broadening, but the overall intensities are comparable with the relative intensities given by the bars.

D. Electronic band structure

Starting from our structure solution for the thin film phase and the structural data of the phase of Campbell *et al.* we calculate and compare the band structures of both polymorphs. The results are shown in the Fig. 5. The subbands corresponding to the uppermost valence band (VB) and lowest conducting band (CB) pair as well as their corresponding DOS are displayed in gray in this figure. We should mention that in the original determination of the structure of Campbell *et al.* a different setup of the unit cell was used. In order to be able to compare both structures, we have chosen another set of basis vectors allowing for a direct comparison with the thin film phase (see Table I).

The most distinct features of the band structures of both polymorphs are summarized in Table III. The band structure of the thin film phase exhibits a more dispersive character. A denser packing of the molecules in the (**ab**) plane leads to stronger intermolecular interaction. Therefore, the bandwidths of both the conduction and the valence bands are significantly enhanced. In particular, we observe a twice as large valence bandwidth compared to the corresponding band of the bulk polymorph. The largest splitting of the VB

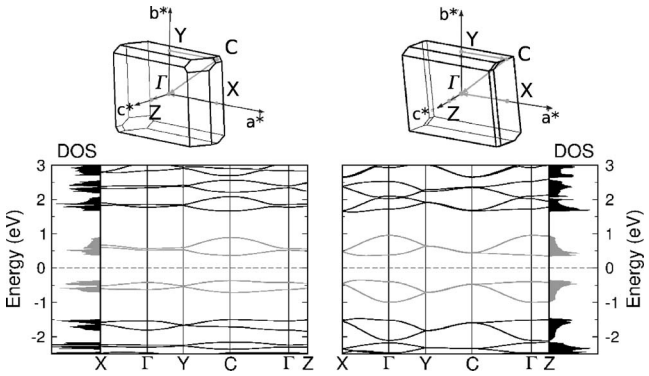

FIG. 5. Calculated band structures for the bulk (left) and thin film (right) pentacene polymorphs. The high-symmetry points in units $(2\pi/a, 2\pi/b, 2\pi/c)$ are $\Gamma=(0,0,0)$, $X=(0.5,0,0)$, $Y=(0,0.5,0)$, $C=(0.5,0.5,0)$, and $Z=(0,0,0.5)$. The Fermi level is indicated by a dashed line. The subbands of the VB and CB as well as their DOS are given in gray. On top the corresponding Brillouin zones are presented.

and CB of the thin film phase is observed at the Γ point, while in bulk pentacene, this is at the *C* point. The top of the valence band of the thin film polymorph is situated in the point (0.7, 0.0, 0.0). It is noteworthy that the Kohn-Sham band gap of the thin film phase (0.70 eV) is only slightly smaller than that of the bulk phase (0.74 eV) for which similar values have been reported previously.[19,20]

V. CONCLUSIONS AND DISCUSSION

In this work, we have provided a structural solution of the pentacene thin film phase by applying a combined experimental and theoretical approach. We have investigated the internal geometry of the pentacene thin film phase by first-principles DFT calculations using experimentally determined lattice parameters. A comparison with the well-known bulk crystal structure as determined by Campbell *et al.* has been made. We found the herringbone angle to be about 54° which is slightly larger than that in the latter structure. The most pronounced difference in the internal geometry, however, is the value of the tilting angle between the long molecular axis and the normal to the (**ab**) plane. While this angle is approximately 3° for the thin film phase, it is about 22° for the bulk polymorph. These findings are in good agreement with another study performed by Yoshida *et al.*[7] They have solved the pentacene thin film phase by x-ray diffraction studies and found lattice parameters very close to those reported by us.

TABLE III. Calculated energy gap and bandwidths of the highest occupied and the lowest unoccupied pairs of bands for both structures. Additionally, the band gaps calculated in the special points Γ and *C* are given.

	Thin film (eV)	Bulk (eV)
Energy gap	0.70	0.74
Bandwidth		
VB	0.64	0.34
CB	0.62	0.53
Band gap at points		
Γ	0.77	0.93
C	0.90	0.89

Their theoretical investigations of the internal molecular geometry by means of an empirical force field method revealed a herringbone angle of 50°, and tilting angles 5.7° and 6.8°, respectively. The deviations from our results may be explained by the distinct theoretical approaches.

In the thin film phase, the tilting angle is only 3°, i.e., the molecules are standing almost upright within one pentacene layer. As a consequence there is enhanced intermolecular $\pi-\pi$ overlap leading to more dispersive valence and conducting bands and lower values of the effective hole and electron masses. For instance, the bandwidth of the topmost valence band is twice as large in the thin film phase as compared to the single crystal structure of Campbell *et al.* These findings are important for understanding the electro-optical properties of devices based on pentacene thin films. Since the active channel in these organic field effect transistors most likely is composed of the pentacene molecules in the thin film phase, the structural solution and the corresponding electronic properties of this phase provided herein will be highly relevant. Therefore, attempts to understand the charge transport in pentacene should start from the correct underlying structure.

ACKNOWLEDGMENTS

The work was supported by the Austrian Science Fund within the National Science Network "Interface Controlled and Functionalised Organic Films." O.W. and R.R. thank the Cornell High Energy Synchrotron Source (CHESS) for provision of synchrotron radiation. The thin film sample was provided by B. Stadlober and A. Haase, Institute of Nanostructures and Photonics, Joanneum Research, Styria, Austria.

*dmitrii.nabok@mu-leoben.at
†http://mu-leoben.at/amadm/

[1] C. D. Dimitrakopoulos and D. J. Mascaro, IBM J. Res. Dev. **45**, 11 (2001).
[2] C. C. Mattheus, A. B. Dros, J. Baas, G. T. Oostergetel, A. Meetsma, J. L. De Boer, and T. T. M. Palstra, Synth. Met. **138**, 475 (2002).
[3] C. C. Mattheus, G. A. de Wijs, R. A. de Groot, and T. T. M. Palstra, J. Am. Chem. Soc. **125**, 6323 (2003).
[4] R. B. Campbell, J. M. Robertson, and J. Trotter, Acta Crystallogr. **15**, 289 (1962).
[5] D. Holmes, S. Kumaraswamy, A. J. Matzger, and K. P. Vollhardt,

Chem.-Eur. J. **5**, 3399 (1999).
[6] T. Siegrist, C. Kloc, J. H. Schœn, B. Batlogg, R. C. Haddon, S. Berg, and G. A. Thomas, Angew. Chem., Int. Ed. **40**, 1732 (2001).
[7] H. Yoshida, K. Inaba, and N. Sato, Appl. Phys. Lett. **90**, 181930 (2007).
[8] S. Schiefer, M. Huth, A. Dobrinevski, and B. Nickel, J. Am. Chem. Soc. **129**, 10316 (2007).
[9] S. Kowarik, A. Gerlach, W. Leitenberger, J. Hu, G. Witte, C. Wöll, U. Pietsch, and F. Schreiber, Thin Solid Films **515**, 5606 (2007).
[10] A. C. Mayer, A. Kazimirov, and G. G. Malliaras, Phys. Rev. Lett. **97**, 105503 (2006).
[11] C. D. Dimitrakopoulos, A. R. Brown, and A. Pomp, J. Appl. Phys. **80**, 2501 (1996).
[12] D. J. Gundlach, T. N. Jackson, D. G. Schlom, and S. F. Nelson, Appl. Phys. Lett. **74**, 3302 (1999).
[13] G. Heimel, P. Puschnig, M. Oehzelt, K. Hummer, B. Koppelhuber-Bitschnau, F. Porsch, C. Ambrosch-Draxl, and R. Resel, J. Phys.: Condens. Matter **15**, 3375 (2003).
[14] G. Heimel, K. Hummer, C. Ambrosch-Draxl, W. Chunwachirasiri, M. J. Winokur, M. Hanfland, M. Oehzelt, A. Aichholzer, and R. Resel, Phys. Rev. B **73**, 024109 (2006).
[15] M. Oehzelt, K. Weinmeier, G. Heimel, P. Puschnig, R. Resel, C. Ambrosch-Draxl, F. Porsch, and A. Nakayama, High Press. Res. **22**, 343 (2002).
[16] M. Oehzelt, A. Aichholzer, R. Resel, G. Heimel, E. Venuti, and R. G. Della Valle, Phys. Rev. B **74**, 104103 (2006).
[17] K. Doi, K. Yoshida, H. Nakano, A. Tachibana, T. Tanabe, and Y. Kojima, J. Appl. Phys. **98**, 113709 (2005).
[18] P. Parisse, L. Ottaviano, B. Delley, and S. Picozzi, J. Phys.: Condens. Matter **19**, 106209 (2007).
[19] K. Hummer and C. Ambrosch-Draxl, Phys. Rev. B **72**, 205205 (2005).
[20] M. L. Tiago, J. E. Northrup, and S. G. Louie, Phys. Rev. B **67**, 115212 (2003).
[21] M. Oehzelt, G. Heimel, R. Resel, P. Puschnig, K. Hummer, C. Ambrosch-Draxl, K. Takemura, and A. Nakayama, J. Chem. Phys. **119**, 1078 (2003).
[22] B. Stadlober, U. Haas, H. Maresch, and A. Haase, Phys. Rev. B **74**, 165302 (2006).
[23] D.-M. Smilgies, D. R. Blasini, S. Hotta, and H. Yanagi, J. Synchrotron Radiat. **12**, 807 (2005).
[24] www.pwscf.org and www.quantum-espresso.org
[25] D. Vanderbilt, Phys. Rev. B **41**, R7892 (1990).
[26] J. P. Perdew, K. Burke, and M. Ernzerhof, Phys. Rev. Lett. **77**, 3865 (1996).
[27] H. J. Monkhorst and J. D. Pack, Phys. Rev. B **13**, 5188 (1976).
[28] P. E. Blöchl, O. Jepsen, and O. K. Andersen, Phys. Rev. B **49**, 16223 (1994).
[29] G. R. Desiraju and A. Gravezzotti, Acta Crystallogr., Sect. B: Struct. Crystallogr. Cryst. Chem. **45**, 473 (1989).
[30] K. Hummer, P. Puschnig, and C. Ambrosch-Draxl, Phys. Rev. B **67**, 184105 (2003).
[31] J. Puigdollers, C. Voz, A. Orpella, I. Martin, M. Vetter, and R. Alcubilla, Thin Solid Films **427**, 367 (2003).
[32] T. Kakudate, N. Yoshimoto, and Y. Saito, Appl. Phys. Lett. **90**, 081903 (2007).
[33] R. Ruiz, A. C. Mayer, G. G. Malliaras, B. Nickel, G. Scoles, A. Kazimirov, H. Kim, R. L. Headrick, and Z. Islam, Appl. Phys. Lett. **85**, 4926 (2004).
[34] H. Yoshida and N. Sato, Appl. Phys. Lett. **89**, 101919 (2006).
[35] S. E. Fritz, S. M. Martin, C. D. Frisbie, M. D. Ward, and M. F. Toney, J. Am. Chem. Soc. **126**, 4084 (2004).
[36] V. Vand, Acta Crystallogr. **1**, 109 (1948).
[37] J. S. Wu and C. H. Spence, J. Appl. Crystallogr. **37**, 78 (2004).
[38] We expect that the mosaicity should play only a minor role since the out-of-plane rocking curves of our pentacene film are as small as those from single crystals. Since this does, however, not need to be the general case, one should keep this issue in mind in future grazing incidence diffraction studies.